Nontrivial magnetoresistive behavior of a single-wall carbon nanotube with an attached molecular magnet

Anna Płomińska[*] and Ireneusz Weymann[†]
Faculty of Physics, Adam Mickiewicz University, ul. Umultowska 85, 61-614 Poznań, Poland
(Received 14 September 2015; published 16 November 2015)

The spin-resolved transport properties of a single-wall carbon nanotube quantum dot, with an attached single molecular magnet, are studied theoretically. With the aid of the real-time diagrammatic technique in the lowest-order perturbation expansion with respect to the tunnel coupling, the current, differential conductance, and the tunnel magnetoresistance (TMR) are determined in both the linear and nonlinear response regimes. It is shown that transport properties depend greatly on both the shell filling sequence of the carbon nanotube and the type of exchange interaction between the molecular magnet and nanotube. This results in highly nontrivial behavior of the TMR, which is especially visible in the low bias voltage regime. Depending on the gate voltage and parameters of the system, we find transport regimes where either a greatly enhanced or negative TMR develops. The mechanism leading to such behavior is associated with nonequilibrium spin accumulation, which builds up in the antiparallel magnetic configuration of the device. We show that it is crucial whether the spin accumulation occurs in the highest-weight spin states or in states with lower spin values. While in the former case it leads to enhanced TMR, in the latter case it may result in negative tunnel magnetoresistance. In addition, we analyze how the above effects depend on the magnitude of the molecular magnet's spin, and show that this dependence is generally nonmonotonic.

DOI: 10.1103/PhysRevB.92.205419 PACS number(s): 72.25.−b, 73.63.Kv, 75.50.Xx, 85.75.−d

I. INTRODUCTION

Rapid progress in nanotechnology has enabled implementation and measurements of individual nanoscale objects, such as quantum dots or molecules coupled to external leads, with controllable parameters [1–6]. Transport properties of such nanostructures depend greatly on the quality of contact to external leads and on the nanostructure's intrinsic properties and parameters. When the coupling is relatively weak, single-electron tunneling and Coulomb blockade effects become visible in transport characteristics [1], whereas in the case of strong coupling, the electronic correlations can give rise to the Kondo effect [7–9]. Further interesting phenomena arise when external leads are ferromagnetic [10–15]. In magnetic nanostructures the magnitude of the flowing current is determined by the magnetic configuration of the device. Due to the mismatch in the spin-resolved densities of states, the current is usually larger in the case of parallel magnetic configuration compared to an antiparallel one, leading to spin-valve-like behavior [16]. In fact, nanoscale spin valves, built from dots or molecules, can be regarded as basic building blocks of modern spin nanoelectronics and molecular spintronics, which nowadays are attracting considerable attention [17–19].

While in simple quantum dot spin valves a positive tunnel magnetoresistance (TMR) was predicted [20,21], more complex behavior can be expected in molecular spin valves [22]. In particular, recent theoretical studies have shown that in the case of magnetic molecules with large spin, such as single molecular magnets (SMM) [23–25], magnetoresistive properties of the device depend strongly on the intrinsic properties of SMM, leading to more complex spin-resolved transport characteristics [26–34]. Moreover, it has been demonstrated in a system built from a carbon nanotube (CNT) coupled to two single molecular magnets that not only the magnetic configuration of external leads can affect the transport properties, but also mutual alignment of SMMs' spins can play a similar role [5]. In such supramolecular spin valves, the conductance through the system can be then controlled by changing the alignment of SMMs' spins in an external magnetic field. All these clearly indicate that there is a lot of interest in various molecular spin valve devices. This is stimulated by the fact that, besides fascinating physics, such nanostructures are potential candidates for future applications in, e.g., information storage and processing technologies [35,36]. Nevertheless, despite great progress in both theoretical and experimental investigations, there are still some aspects that need further exploration.

In this paper we thus analyze the spin-resolved transport properties of a single-wall carbon nanotube, with an attached single molecular magnet, coupled to external leads. The considered system bears a strong resemblance to a recently implemented supramolecular spin valve [5]. Here, however, instead of two SMMs attached to CNT, only one is considered. In this regard, the present analysis can be viewed as an intermediate step in understanding more complex transport behavior of supramolecular spin valves. As shown in the following, it turns out that transport properties of CNT even with one single molecular magnet exhibit many nontrivial effects, such as, e.g., great enhancement of the TMR or its suppression and sign change. While transport through SMMs or CNTs coupled to external ferromagnetic leads have already been studied recently [22,37–44], spin-resolved transport characteristics of complex CNT-SMM molecules remain still rather unexplored. Filling this gap is therefore the main goal of this work.

To perform the calculations, we employ the real-time diagrammatic technique in the lowest order of perturbative expansion with respect to the tunnel coupling to external

[*]anna.plominska@amu.edu.pl
[†]weymann@amu.edu.pl

leads [45–47]. We determine the bias and gate voltage dependence of the current, differential conductance, and the tunnel magnetoresistance in the case of both ferromagnetic and antiferromagnetic exchange interaction between the nanotube and single molecular magnet. In particular, we study how the transport properties depend on the sequence of ground states of isolated carbon nanotube, which in a two-electron state can be either in a spin singlet or a spin triplet state, depending on CNT's parameters [48–51]. We predict a highly nontrivial behavior of the TMR, which depends on the nanotube ground state sequence and is determined by the type of exchange interaction between CNT and SMM and the magnitude of SMM's spin. Moreover, our analysis shows that bias spectroscopy can provide additional information about the exchange interaction between CNT and SMM and internal parameters of the nanosystem.

The paper is organized in the following manner. Section II is devoted to theoretical formulation of the problem, where the model and Hamiltonian of the system (Sec. II A), calculation method (Sec. II B), and system parameters (Sec. II C) are described. The main part of the paper is presented in Sec. III, which contains numerical results and their discussion. First, the case when the two-electron ground state of nanotube is spin singlet is considered (Sec. III A), and then the case of spin triplet is analyzed (Sec. III B). Finally, concluding remarks can be found in Sec. IV.

II. THEORETICAL DESCRIPTION

A. Model and Hamiltonian of the system

The considered system consists of a single-wall carbon nanotube quantum dot with an attached magnetic molecule, such as a single molecular magnet, characterized by the spin operator **S**, see Fig. 1. The exchange coupling between the molecule and nanotube is denoted by J_S and can be either of ferromagnetic or antiferromagnetic type. Such a nanostructure is coupled to the left and right ferromagnetic leads with coupling strengths Γ_L^σ and Γ_R^σ, respectively. The magnetizations of the leads are assumed to form either parallel or antiparallel magnetic configuration, as indicated in Fig. 1, and the easy axis of the molecule is assumed to coincide with the magnetization of the left electrode. The magnetic configuration of the device can be changed upon applying a small external magnetic field, provided that the two ferromagnets have different coercive fields. Such a magnetic field is assumed to have negligible effect on the energy levels of the considered molecular system.

The total Hamiltonian of the system can be written as

$$H = H_{\rm Lead} + H_{\rm Mol} + H_{\rm Tun}, \tag{1}$$

where

$$H_{\rm Lead} = \sum_{rk\sigma} \varepsilon_{rk\sigma} c^\dagger_{rk\sigma} c_{rk\sigma} \tag{2}$$

describes the noninteracting electrons in the leads, with $c^\dagger_{rk\sigma}$ being an operator for creating a spin-σ electron with momentum k in electrode r ($r = L, R$) of energy $\varepsilon_{rk\sigma}$. The second term of the total Hamiltonian describes the molecular part of the system and is given by [22,48,52,53]

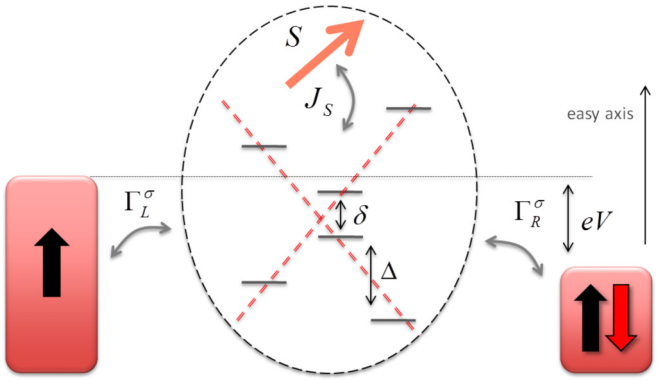

FIG. 1. (Color online) Schematic of the considered system. It consists of a single-wall carbon nanotube quantum dot, with an attached single molecular magnet (with coupling J_S) characterized by the spin operator **S**, coupled to external ferromagnetic leads with coupling strengths Γ_L^σ and Γ_R^σ. The easy axis of the molecule coincides with the magnetization of the left lead, while the magnetization of the right lead can change direction, resulting in two magnetic configurations: the parallel and antiparallel one. The two subbands of the nanotube are sketched with dashed lines, δ denotes the energy mismatch between the subbands, while Δ is the nanotube level spacing. A voltage drop V is applied symmetrically between the leads.

$$H_{\rm Mol} = \sum_{\alpha j\sigma} \varepsilon_{\alpha j} n_{\alpha j\sigma} + \frac{E_C}{2} N^2 + J N_\uparrow N_\downarrow - J_S \mathbf{S}\cdot\mathbf{s} - D S_z^2, \tag{3}$$

where the first three terms model the carbon nanotube quantum dot, the fourth one describes the exchange coupling between the nanotube and molecular magnet, while the last term accounts for the molecule's magnetic anisotropy. The carbon nanotube is characterized by two spin-degenerate subbands of linear dispersion, as sketched in Fig. 1. Its discrete energy levels are denoted by $\varepsilon_{\alpha j}$, with $\varepsilon_{\alpha j} \equiv \varepsilon + \delta(\alpha - 1) + \Delta(j - 1)$, where δ is the energy mismatch between the subbands of the nanotube denoted by α ($\alpha = 1,2$), Δ is the level spacing, and j numbers the energy levels belonging to a given subband. The corresponding particle number operator of the nanotube is denoted by $n_{\alpha j\sigma} = d^\dagger_{\alpha j\sigma} d_{\alpha j\sigma}$, with $d^\dagger_{\alpha j\sigma}$ creating a spin-σ electron in energy level j of subband α, and $N_\sigma = \sum_{\alpha j} n_{\alpha j\sigma}$, with $N = N_\uparrow + N_\downarrow$. The charging energy of the nanotube is denoted by E_C, while J is the intrinsic exchange interaction in the nanotube [48–51]. On the other hand, J_S describes the exchange coupling between molecular magnet and nanotube, with **S** denoting the spin operator of the former, while $\mathbf{s} = \frac{1}{2}\sum_{\alpha j}\sum_{\sigma\sigma'} d^\dagger_{\alpha j\sigma} \vec{\sigma}_{\sigma\sigma'} d_{\alpha j\sigma'}$ is the spin operator of the latter, with $\vec{\sigma}$ being the vector of Pauli spin matrices. Finally, D stands for the uniaxial magnetic anisotropy of SMM and S_z is the zth component of the spin operator **S**. The magnitude of the SMM and CNT spins is denoted by S and s, respectively.

The last term of the total Hamiltonian (1) takes into account tunneling processes between the molecule and the

leads

$$H_{\rm Tun} = \sum_{r\alpha j} t_{r\alpha j} \sum_{k\sigma} (c^{\dagger}_{rk\sigma} d_{\alpha j\sigma} + d^{\dagger}_{\alpha j\sigma} c_{rk\sigma}), \tag{4}$$

where the tunnel matrix elements between the jth level of the carbon nanotube belonging to subband α and the rth lead are described by $t_{r\alpha j}$. The coupling strength between the leads and the corresponding levels of the nanotube is given by $\Gamma^{\sigma}_{r\alpha j} = 2\pi\rho^{\sigma}_{r} t^{2}_{r\alpha j}$, where ρ^{σ}_{r} denotes the spin-dependent density of states of lead r. The coupling can be expressed in terms of the spin polarization of the leads $p_r = (\rho^{\uparrow}_r - \rho^{\downarrow}_r)/(\rho^{\uparrow}_r + \rho^{\downarrow}_r)$, as $\Gamma^{\sigma}_{r\alpha j} = (1 \pm p_r)\Gamma_{r\alpha j}$, with $\Gamma_{r\alpha j} = (\Gamma^{\uparrow}_{r\alpha j} + \Gamma^{\downarrow}_{r\alpha j})/2$. In this work the system is assumed to be symmetric, i.e., $p_r \equiv p$, $\Gamma_{r\alpha j} \equiv \Gamma$, and the voltage drop is applied symmetrically between the leads.

We note that the Hamiltonian of the isolated SMM-CNT molecule is not diagonal in the eigenbasis spanned by $\{|\alpha,j,q,\sigma\rangle \otimes |S,S_z\rangle\}$, where $|\alpha,j,q,\sigma\rangle$ ($|S,Sz\rangle$) are the eigenstates of the nanotube (molecular magnet) itself, with q denoting charge in level j for spin σ belonging to subband α. Therefore, we first perform numerical diagonalization of $H_{\rm Mol}$ to find its eigenstates and eigenenergies $H_{\rm Mol}|\chi\rangle = \varepsilon_{\chi}|\chi\rangle$, where $|\chi\rangle$ denotes a many-body eigenstate of $H_{\rm Mol}$ and ε_{χ} is the respective eigenenergy. Note that the dimension of the full molecule's Hilbert space is $4^{(N_1+N_2)}(2S+1)$, where N_{α} is the number of states in subband α. We also notice that, although only carbon nanotube is coupled directly to the leads, due to the exchange interaction J_S, tunneling processes occur through molecular states $|\chi\rangle$ of the whole molecular magnet-carbon nanotube system.

In our analysis we focus on a relatively low bias voltage range $|eV| < \Delta$, therefore in calculations we take into account two orbital levels of the nanotube, each belonging to a different subband, i.e., $j = 1$ and $\alpha = 1,2$. It is then convenient to relabel the energy levels as $\varepsilon_{11} \equiv \varepsilon$ and $\varepsilon_{21} \equiv \varepsilon + \delta$. The dimension of the local Hilbert space is reduced to $4^2(2S+1)$. Since the Hamiltonian commutes with total spin zth component $S^{\rm tot}_z = s_z + S_z$, and nanotube particle number operators, we can use those quantum numbers to label the molecular states of the Hamiltonian $H_{\rm Mol}$, $|\chi\rangle \equiv |q_1,q_2,S^{\rm tot}_z\rangle$, where q_j denotes charge on the jth orbital level. Note that this notation is not entirely unique, since there may be more states with the same quantum numbers, however, since in the following discussion we will consider mainly the lowest energy states, this notation is sufficient to describe all the interesting transport properties of the system.

B. Method of calculations

In order to determine the transport characteristics of the considered system we employ the real-time diagrammatic technique [45–47]. This approach relies on a systematic perturbation expansion of occupation probabilities and operators of interest with respect to the coupling strength Γ. The calculation starts with the determination of self-energies in a given order of expansion, which are then used to determine the density matrix elements and, finally, the current flowing through the system. In these considerations we assume that the molecule is weakly coupled to external leads, such that transport occurs mainly due to incoherent sequential tunneling processes. Therefore, we consider only the lowest-order terms of perturbative expansion. Moreover, here we also adopt a recently introduced notation, which allows us to express the occupation probabilities and the current in terms of appropriate self-energy matrices $\mathbf{W}$ and $\mathbf{W}^{\rm I}$, the elements of which describe transitions between corresponding many-body states $|\chi\rangle$ [46,47].

The elements of matrix $\mathbf{W}$ are given by $W_{\chi\chi'} = W^{\rm L}_{\chi\chi'} + W^{\rm R}_{\chi\chi'}$, where [54]

$$W^{r}_{\chi\chi'} = 2\pi \sum_{\sigma} \rho^{\sigma}_{r} \left\{ f_r(\varepsilon_{\chi} - \varepsilon_{\chi'}) \left| \sum_{\alpha j} t_{r\alpha j} \langle \chi | d^{\dagger}_{j\sigma} | \chi' \rangle \right|^2 + [1 - f_r(\varepsilon_{\chi'} - \varepsilon_{\chi})] \left| \sum_{\alpha j} t_{r\alpha j} \langle \chi | d_{j\sigma} | \chi' \rangle \right|^2 \right\},$$

for $\chi \neq \chi'$ and $W^{r}_{\chi\chi} = -\sum_{\chi' \neq \chi} W^{r}_{\chi'\chi}$, with $f_r(\varepsilon) = 1/[e^{(\varepsilon-\mu_r)/T} + 1]$ being the Fermi-Dirac distribution function and μ_r denoting the electrochemical potential of lead r. Knowing the self-energy matrix $\mathbf{W}$, one can calculate the steady-state occupation probabilities P_{χ} of many-body states $|\chi\rangle$ from the equation [46,47]

$$(\mathbf{WP}) = 0, \tag{5}$$

together with the normalization condition $\mathrm{Tr}(\mathbf{P}) = 1$, where $\mathbf{P}$ denotes vector of probabilities. The current flowing through the system can be then found from [46,47]

$$I = \frac{e}{2\hbar} \mathrm{Tr}\{\mathbf{W}^{I}\mathbf{P}\}, \tag{6}$$

where the elements of self-energy matrix $\mathbf{W^I}$ are defined as [54]

$$W^{\rm I}_{\chi\chi'} = [\Theta(N_{\chi'} - N_{\chi}) - \Theta(N_{\chi} - N_{\chi'})]\left(W^{\rm R}_{\chi\chi'} - W^{\rm L}_{\chi\chi'}\right),$$

with N_{χ} denoting the number of electrons in state $|\chi\rangle$ and $\Theta(N)$ is the step function.

C. Quantities of interest and parameters of the system

In this paper we will in particular study how the spin-resolved transport properties of the system change when the magnetic configuration is varied between the parallel and antiparallel alignment. This change can be described by the tunnel magnetoresistance, which is defined as [55]

$$\mathrm{TMR} = \frac{I^{\rm P} - I^{\rm AP}}{I^{\rm AP}}, \tag{7}$$

where $I^{\rm P}$ ($I^{\rm AP}$) denotes the current flowing in the parallel (antiparallel) magnetic configuration of the system.

To model the carbon nanotube we take $E_C \equiv 1$ to be the energy unit and assume $J = 0.4$ [49,50]. Since δ is a rather arbitrary parameter, which describes the mismatch between the subbands of the nanotube that can be caused by, e.g., the interfaces, we will analyze the transport properties for two values of δ: $\delta = 0$ and $\delta = 0.8$. In the former case, $\delta < J$, when the nanotube is occupied by two electrons, its ground state is spin triplet, however, in the latter case ($\delta > J$) the ground state becomes spin singlet [50]. As will be shown in the next section,

the sequence of ground states of an isolated nanotube has a strong impact on the spin-resolved transport characteristics. On the other hand, the single molecular magnet is described by a hypothetical spin $S = 2$ and we assume $D = 0.1$ and $|J_S| = 0.15$. However, we will also consider how the magnitude of the SMM's spin S affects the transport behavior of the system. Note also that J_S can be of either ferromagnetic ($J_S > 0$) or antiferromagnetic ($J_S < 0$) type. Moreover, in calculations we assume $T = 0.05$, $\Gamma = 0.01$, and the lead's spin polarization $p = 0.5$.

III. RESULTS AND DISCUSSION

In this section we present and discuss the numerical results on the current and differential conductance in the parallel and antiparallel magnetic configurations as well as the resulting tunnel magnetoresistance as a function of the bias and gate voltages. Since the position of the molecule's orbital levels can be changed upon application of a gate voltage, the dependence on ε effectively resembles the dependence on the gate voltage. Moreover, since single-wall carbon nanotube quantum dots exhibit four-electron periodicity as a function of gate voltage [49–51], by considering two orbital levels we are able to analyze one period of this oscillatory behavior. Transport characteristics of the system are expected to be periodic with the gate voltage. Let us first analyze the case when $\delta > J$, such that the two-electron ground state of the isolated nanotube is spin singlet.

A. Results in the case of $\delta > J$

When $\delta > J$, the isolated nanotube has the following sequence of spin ground states $s = 0, \frac{1}{2}, 0, \frac{1}{2}, 0$ when changing its occupancy from zero to four, that is, the ground state is spin singlet for even occupancy and spin doublet for odd occupancy. Of course the total spin of the CNT-SMM system is modified by the presence of the molecular magnet's spin S and depends on the sign of exchange interaction J_S. If one assumes $D(2S-1) \gg T$, such that SMM is in spin states of the lowest energy and J_S is of ferromagnetic type, then the total spin of the system is simply given by $S_{\rm tot} = S + s$. On the other hand, antiferromagnetic exchange coupling tends to lower the total spin. In the following we analyze the transport properties in the case of ferromagnetic J_S, $J_S > 0$, and then proceed to the case of antiferromagnetic J_S, $J_S < 0$.

1. *Ferromagnetic exchange interaction J_S*

For $J_S > 0$, when assuming $D(2S-1) \gg T$ and $\delta - J \gg T$, one can estimate the parameters for which the ground state of the molecular system changes as a function of ε. These energies correspond to resonances which appear in the gate voltage dependence of the linear conductance. They occur whenever $\varepsilon = \varepsilon_{qq+1}$, where $q = q_1 + q_2$ denotes the charge state of the system and ε_{qq+1} is given by

$$\varepsilon_{01} = -\frac{E_C}{2} + \frac{J_S S}{2},$$
$$\varepsilon_{12} = -\frac{3E_C}{2} - J - \frac{J_S S}{2},$$
$$\varepsilon_{23} = -\frac{5E_C}{2} - \delta - J + \frac{J_S S}{2},$$
$$\varepsilon_{34} = -\frac{7E_C}{2} - \delta - 2J - \frac{J_S S}{2}. \quad (8)$$

In this notation, e.g., ε_{01} denotes the energy for which the charge states with zero and one electron are degenerate. This is associated with a first resonance in the linear conductance when lowering the level position ε. The middle of the four-electron sequence occurs for $\varepsilon_m = (\varepsilon_{12} + \varepsilon_{12})/2 = -2E_C - J - \delta/2$. For the left-right symmetric system and in the absence of magnetic field, the transport characteristics are symmetric with respect to this point. One can see that the presence of the molecular magnet generally leads to shifting of resonances. In particular, the width of the middle region, where the system is in a two-electron state, becomes decreased with J_S, while the singly occupied region increases with raising J_S. Nevertheless, it needs to be emphasized that besides this effect, the presence of SMM has much stronger influence on the spin states of the system and, thus, on its spin-resolved transport properties, which reveal most pronouncedly in the behavior of TMR. Moreover, the exchange coupling with the molecular magnet can also affect the sequence of ground states of the nanotube. The two-electron state of the nanotube is spin singlet only if $\delta - J > J_S S$. When $\delta - J < J_S S$ (for $J_S > 0$), it is more favorable for the nanotube to be occupied by two electrons on different levels with the same spin, resulting in spin triplet. Thus, the formulas for resonant energies (8) are valid only when $\delta - J > J_S S$.

The bias voltage and level position dependence of the differential conductance in both magnetic configurations and of the TMR in the case of $\delta > J$ and for ferromagnetic exchange coupling J_S is shown in Fig. 2. Figures 2(a) and 2(b) present typical Coulomb stability diagrams of the device. The diamonds at low bias voltage correspond to transport regions where the system is in the Coulomb blockade regime with a fixed number of electrons. The Coulomb blockade can be lifted by either changing the gate voltage to resonance energy or by applying a bias voltage. If, for a given ε, the bias voltage reaches a threshold voltage for sequential tunneling, there is a step in the current which results in peak in the differential conductance. On the other hand, the lines visible for larger voltages are due to various excited states taking part in transport. At low bias voltage, when changing the level position ε, the system becomes consecutively occupied with electrons. The resonances occur at energies given by Eq. (8). The distance between the first and second (and third and fourth) resonance is given by $\varepsilon_{01} - \varepsilon_{12} = E_C + J + J_S S$, while the distance between the second and third resonance is $\varepsilon_{12} - \varepsilon_{23} = E_C + \delta - J_S S$. Thus, by changing either the spin of SMM or its coupling to the nanotube, the size of the Coulomb diamonds becomes modified. In particular, increasing both S and J_S leads to an enlargement of the first and third diamonds, while the middle diamond gets decreased.

We note that in the Coulomb blockade regime at low temperatures the sequential tunneling is suppressed and the dominant contribution to the current comes from cotunneling processes [56,57]. However, for a relatively large ratio of T/Γ, as considered here, one can expect that the rate of thermally activated sequential processes is large enough to

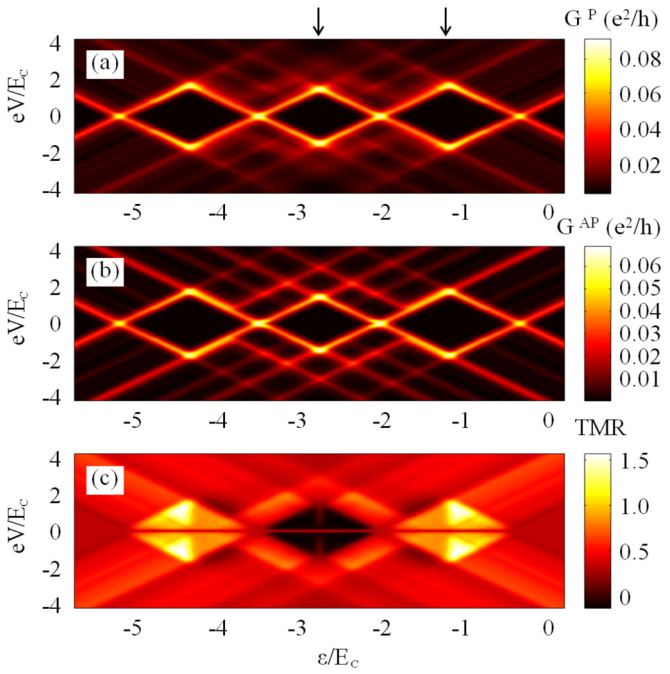

FIG. 2. (Color online) The bias voltage and energy level dependence of the differential conductance in (a) the parallel and (b) antiparallel magnetic configuration and (c) the resulting TMR calculated in the case of ferromagnetic exchange coupling ($J_S > 0$) between the CNT and SMM. The parameters are: $J/E_C = 0.4$, $\delta/E_C = 0.8$, $J_S/E_C = 0.15$, $D/E_C = 0.1$, $T/E_C = 0.05$, $\Gamma/E_C = 0.01$, with $E_C \equiv 1$ the energy unit and $p = 0.5$.

give reasonably good insight into the transport behavior of the system. Nevertheless, some small modification due to cotunneling processes should still be expected [12,39].

As can be seen in Fig. 2, the general structure of the stability diagram is qualitatively similar in both magnetic configurations, since it is mainly determined by the charge states of the system. Nevertheless, some minor differences can still be seen for lines in differential conductance at larger voltages, especially in their intensity, which are due to excited states. However, the main difference between the parallel and antiparallel configuration is related to a change in the magnitude of the conductance, which is generally smaller in the antiparallel configuration compared to the parallel one. This is a direct consequence of the mismatch between the densities of states in the antiparallel configuration where the majority-spin (minority-spin) electrons of one lead tunnel the minority-spin (majority-spin) subband of the other lead. The difference between transport properties in both magnetic configurations is captured by the TMR, the dependence of which on bias and gate voltages is shown in Fig. 2(c). One can see that the TMR takes rather well defined values in-between the lines of the differential conductance. Since each line in dI/dV corresponds to a step in the current, between those lines the current is rather constant and exhibits a plateau, and so does the TMR.

Let us now discuss the behavior of the TMR in more detail. First, general observation is that out of the Coulomb blockade the TMR is always positive and takes values smaller than that predicted by the Julliere model [55] $\mathrm{TMR}^{\mathrm{Jull}} = 2p^2/(1-p^2)$, which is characteristic of a single ferromagnetic tunnel junction, and for assumed spin polarization equals $\mathrm{TMR}^{\mathrm{Jull}} = 2/3$. This is due to the fact that in the considered system the electrons are transferred between the left and right leads through a complex large-spin nano-object and, in addition, sequential tunneling processes are incoherent. This results in spin relaxation and, consequently, one finds TMR smaller than $\mathrm{TMR}^{\mathrm{Jull}}$. We would like to note that a similar tendency has also been observed for carbon nanotubes in the absence of a single molecular magnet [38] and for individual SMMs attached to external ferromagnetic leads [22]. As in the large bias voltage regime the behavior of TMR is rather typical, a completely different situation is observed in the low bias voltage regime where the system is in the Coulomb blockade, see Fig. 2(c). Here the TMR can either take values greatly exceeding the Julliere value or become negative, depending on the occupancy of the nanotube. In particular, in the case of ferromagnetic J_S, we find suppressed TMR for the Coulomb blockade region with two electrons (note that for assumed parameters the isolated nanotube is then in spin singlet state $s = 0$). In this transport regime, the TMR can in fact take negative values. Moreover, for odd occupancy of the nanotube, i.e., when it hosts an unpaired electron ($s = 1/2$), the TMR becomes greatly enhanced, with $\mathrm{TMR} > \mathrm{TMR}^{\mathrm{Jull}}$. Since the behavior of TMR is directly associated with corresponding spin states that are relevant for transport, one can expect that, e.g., changing the type of exchange interaction between the CNT and SMM will have a profound influence on the TMR. This is indeed the case, as we will show in the next sections. We also note that the effect of negative TMR has also been reported in carbon nanotubes in the absence of an additional molecule [13,37,42]. Here, however, negative TMR is exclusively due to the exchange coupling with a single molecular magnet.

To understand the behavior of the TMR depending on the charge state of the nanotube, in Fig. 3 we present the bias voltage dependence of the current, differential conductance, and the TMR for $\varepsilon = \varepsilon_m = -2E_C - J - \delta/2$ ($\varepsilon/E_C = -2.8$) and $\varepsilon = -E_C - J/2$ ($\varepsilon/E_C = -1.2$). These two values correspond to the middle of the second and the first Coulomb diamonds, as marked by vertical arrows in Fig. 2. Let us first discuss the former case. At equilibrium the system is then in a two-electron state, with electrons fully occupying a lower orbital level of the nanotube ($s = 0$), while the molecule is in high spin state. Because there is no external magnetic field, the ferromagnetic ground state of the system is twofold degenerate $|2,0,\pm S\rangle$. In addition, due to finite and relatively large temperature, at equilibrium there is also a small occupation of the excited states $|1,1,\pm S \pm 1\rangle$. With increasing the bias voltage, in the parallel configuration mainly the states $|2,0,\pm S\rangle$ (with equal probabilities) are relevant for transport, until the voltage reaches threshold voltage and more states start participating in the current flow. The situation is completely different in the antiparallel configuration, where a strong nonequilibrium spin accumulation develops. For positive bias voltage (the electrons tunnel from right to left) tunneling of spin-down electrons from the right lead to the molecule is relatively fast, while further tunneling to the left lead is slow. This leads to accumulation of spin-down electrons in the system. As a consequence, one observes large spin

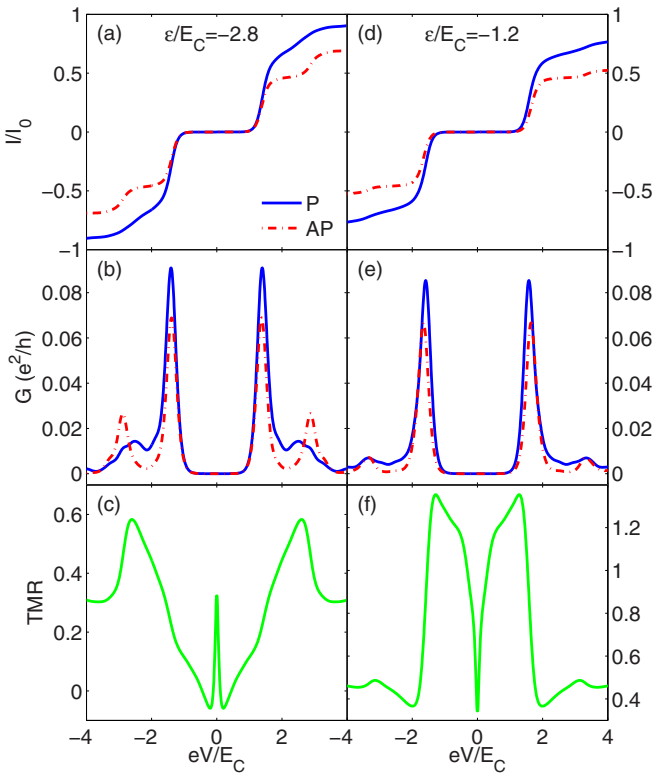

FIG. 3. (Color online) The bias voltage dependence of (a) and (d) the current, (b) and (e) differential conductance in both magnetic configurations, and (c) and (f) the TMR for (left column) $\varepsilon/E_C = -2.8$ and (right column) $\varepsilon/E_C = -1.2$. The other parameters are the same as in Fig. 2.

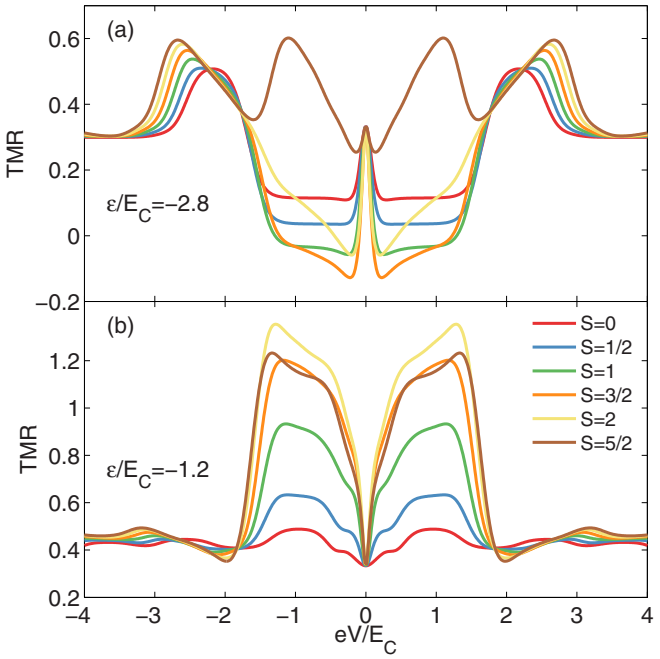

FIG. 4. (Color online) The bias voltage dependence of the TMR in the case of (a) $\varepsilon/E_C = -2.8$ and (b) $\varepsilon/E_C = -1.2$ for different magnitude of the molecular magnet's spin S. The other parameters are the same as in Fig. 2.

accumulation due to enhanced occupation of states $|2,0,-S\rangle$ and $|1,1,-S-1\rangle$. The charge fluctuations between the above states result in increased thermally activated transport through the system, such that the current can become even greater than that in the parallel configuration, leading to negative TMR, see Fig. 3(c). In fact, the maximum spin accumulation occurs for a relatively low bias voltage, which coincides with the minimum in TMR, and then slowly decreases with raising V due to growing occupation of other states. This is seen as a gradual increase of the TMR, until it reaches a local maximum for voltages slightly above the threshold voltage. For negative bias voltage the mechanism is the same, except that the spin accumulation has the opposite sign. Because transport characteristics are symmetric with respect to the bias reversal, from now let us only discuss the results for positive bias voltage.

Opposite to the case shown in the left column of Fig. 3, a completely different situation can be observed when the nanotube occupancy is odd, see the right column of Fig. 3. In this case at equilibrium the system is occupied with equal probability by the states $|1,0,\pm S \pm \frac{1}{2}\rangle$. With increasing the bias voltage in the antiparallel configuration nonequilibrium spin accumulation builds up and the system is in the state $|1,0,-S-\frac{1}{2}\rangle$ with almost full probability. We note that in the parallel configuration, small nonequilibrium spin accumulation is also present, however, both states $|1,0,\pm S \pm \frac{1}{2}\rangle$ have finite and large occupation probabilities. Consequently, because in the antiparallel configuration the system becomes trapped in a single high-spin state, while in the parallel configuration more states are relevant for transport processes, there is a large difference in conductance in both magnetic configurations, with $I^{\mathrm{P}} \gg I^{\mathrm{AP}}$. This results in TMR enhanced much above the Julliere value, see Fig. 3(f).

One could expect that the larger the spin of the molecular magnet the more pronounced spin-resolved effects are revealed in transport properties. A naive and straightforward expectation would be an increase of the TMR when attaching molecules with larger spin S. This is however not necessarily true and, in fact, the situation can be even opposite, i.e., increasing spin S may lead to a lowering of the TMR. Such behavior can be observed in the bias voltage dependence of the TMR calculated for several values of SMM's spin S, ranging from $S = 0$ to $S = \frac{5}{2}$, which is depicted in Fig. 4. The top panel corresponds to the middle of the second diamond, while the bottom panel presents the results in the case when at equilibrium the nanotube is singly occupied. First, we note that the change of S has the most pronounced effect on the TMR in the low bias voltage regime, while for voltages above the threshold voltage the influence of spin S is not that spectacular. Second, although here we present and discuss the data for a hypothetical spin S, the values considered in Fig. 4 can correspond to real physical systems, e.g., molecule of iron $\mathrm{Fe}^{\mathrm{III}}$ has spin $S = 3/2$, while cobalt has spin $S = 1$ [4,58]. Needless to say that there is a large class of SMMs with different spins [23].

When $\varepsilon/E_C = -2.8$, one can see how the TMR becomes suppressed with increasing S. When $S \leqslant \frac{1}{2}$, the TMR is positive in the whole range of bias voltage, see Fig. 4(a). However, when $S > \frac{1}{2}$, negative TMR develops in some range

of the bias voltage. Interestingly, negative TMR is present only for $1 \leqslant S \leqslant 2$ and for $S = \frac{5}{2}$ the TMR again becomes positive in the whole range of the bias voltage considered. The mechanism leading to the suppression of TMR is the same as discussed earlier, the main difference is in the magnitude of spin S, therefore it will not be repeated here. Instead, let us focus on the increase of the TMR with raising S. It turns out that this effect is related to a decrease in energy difference between the twofold degenerate ground state $|2,0,\pm S\rangle$ and excited states $|1,1,\pm S \pm 1\rangle$. For $S = \frac{5}{2}$, these excited states have relatively high occupation probability even at equilibrium. This leads to the situation that despite strong nonequilibrium spin accumulation in the antiparallel configuration, in the parallel configuration transport processes are more effective due to finite occupation of the above four states. Note that for smaller spin S, e.g., $S = 2$, in the parallel configuration mainly the states $|2,0,\pm S\rangle$ are relevant in the low bias voltage range.

A nonmonotonic dependence of the TMR on the magnitude of molecule' spin S can be also seen in the case when the nanotube is occupied by a single electron at equilibrium, see Fig. 4(b). Here one can observe gradual enhancement of the TMR with increasing S, however, for the largest value of S considered here, an opposite trend can be seen—the TMR becomes then slightly lowered. The mechanism leading to an increase of the TMR with spin S is related to the fact that in the parallel configuration the four states $|1,0,\pm S \pm \frac{1}{2}\rangle$ and $|1,0,\pm S \mp \frac{1}{2}\rangle$ are relevant for transport, while in the antiparallel configuration mainly the state $|1,0,-S-\frac{1}{2}\rangle$ is active. Moreover, occupation probability of this state increases with raising S and for $S \geqslant 2$ it is essentially equal to unity. A small decrease of the TMR visible for $S = \frac{5}{2}$ is due to the fact that in the parallel configuration only the spin highest-weight states $|1,0,\pm S \pm \frac{1}{2}\rangle$ become relevant and, thus, the number of possible states for thermally activated transport is reduced. This results in a small suppression of the TMR compared to the case of $S = 2$, see Fig. 4(b), and to related nonmonotonic dependence of TMR on the magnitude of the SMM's spin S.

2. *Antiferromagnetic exchange interaction J_S*

We now analyze how the spin-resolved transport characteristics change when the exchange coupling between the nanotube and molecular magnet is of antiferromagnetic type $J_S < 0$. The bias and gate voltage dependence of the differential conductance in both magnetic configurations and the TMR is shown in Fig. 5. First of all, one can note that the size of the Coulomb diamonds is now slightly changed. This is simply related to the fact that the ground state of the system is no longer given by spin states of highest weight. Instead, depending on the nanotube's occupancy, antiferromagnetic exchange coupling can lead to lowering of the total spin by $s = \frac{1}{2}$ or even $s = 1$ when the nanotube is doubly occupied by a triplet state. Moreover, differences can also be seen in lines in differential conductance for higher voltages due to excited states, see Figs. 5(a) and 5(b). In a similar way, as done in the previous section, one can estimate the energies at which the resonant peaks in linear conductance appear, corresponding to the degeneracy between consecutive charge states. These

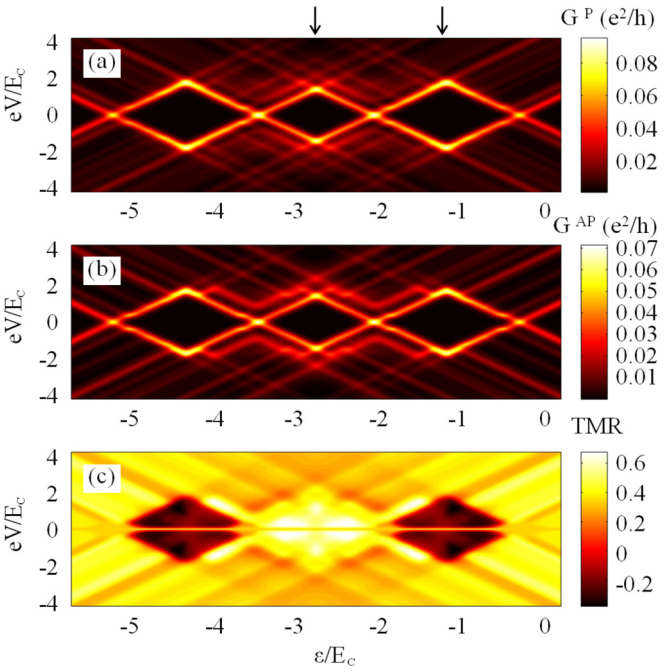

FIG. 5. (Color online) The same as in Fig. 2 calculated in the case of antiferromagnetic exchange coupling ($J_S < 0$) between the molecular magnet and the nanotube, $J_S/E_C = -0.15$.

energies are now given by

$$\begin{aligned}
\varepsilon_{01} &= -\frac{E_C}{2} + \frac{|J_S|}{4} - \frac{\Delta\varepsilon}{2},\\
\varepsilon_{12} &= -\frac{3E_C}{2} - J - \frac{|J_S|}{4} + \frac{\Delta\varepsilon}{2},\\
\varepsilon_{23} &= -\frac{5E_C}{2} - \delta - J + \frac{|J_S|}{4} - \frac{\Delta\varepsilon}{2},\\
\varepsilon_{34} &= -\frac{7E_C}{2} - \delta - 2J - \frac{|J_S|}{4} + \frac{\Delta\varepsilon}{2},
\end{aligned} \tag{9}$$

with $\Delta\varepsilon = (2S-1)D - [D(D+|J_S|)(2S-1)^2 + (J_S/2)^2 (2S+1)^2]^{1/2}$ [22]. Note that the middle of the stability diagram, which is given by ε_m, is still the same as in the case of $J_S > 0$ and only the size of diamonds is modified. Nevertheless, as far as the behavior of TMR is considered, the changes are more dramatic. In particular, the situation is now just the opposite, i.e., we find negative TMR in transport regime where the nanotube is oddly occupied at equilibrium, while in the doubly occupied regime the TMR is positive and its magnitude is not as large as in the case of ferromagnetic J_S (for the oddly occupied system). To understand this behavior, in Fig. 6 we present the relevant cross sections of Fig. 5 (indicated by arrows) for Coulomb blockades with one and two electrons. Let us first focus on the latter case.

At equilibrium, the ground state of the system is twofold degenerate $|2,0,\pm S\rangle$. However, due to finite temperature, there is also relatively high occupation probability of excited states $|1,1,\pm S \mp 1\rangle$. In the parallel configuration these four states are relevant for transport in the Coulomb blockade regime. On the other hand, in the case of antiparallel configuration, nonequilibrium spin accumulation sets in and the occupation of two states $|2,0,-S\rangle$ and $|1,1,-S+1\rangle$ is increased. Because

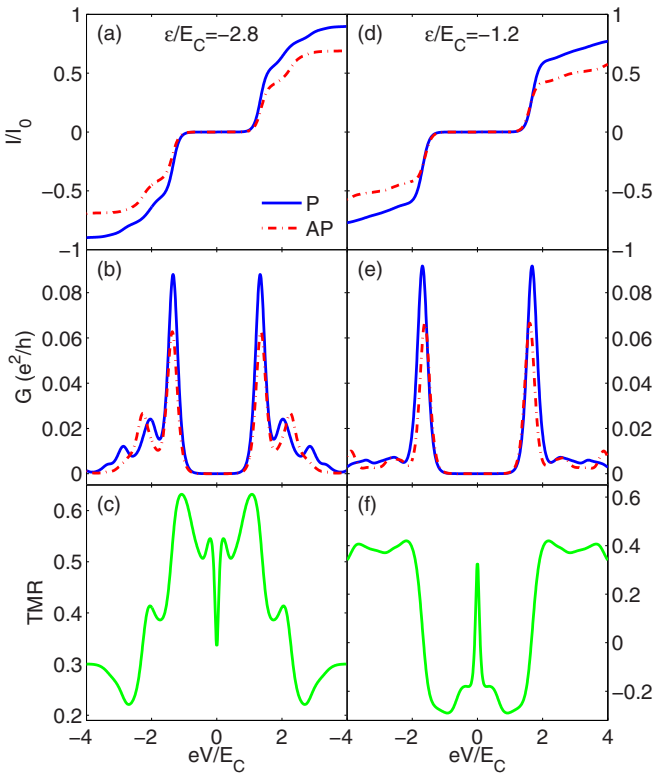

FIG. 6. (Color online) The bias voltage dependence of (a) and (d) the current, and (b) and (e) differential conductance in both magnetic configurations, as well as (c) and (f) the TMR for (left column) $\varepsilon/E_C = -2.8$ and (right column) $\varepsilon/E_C = -1.2$. The other parameters are the same as in Fig. 2 with $J_S/E_C = -0.15$.

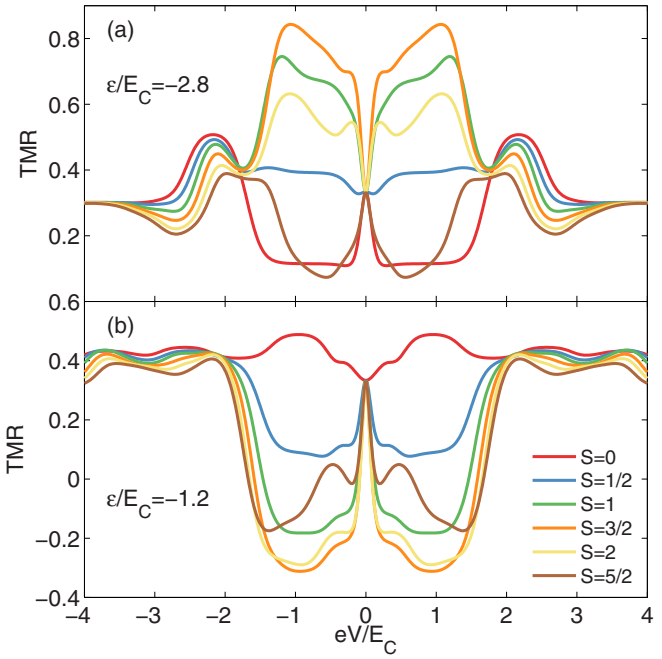

FIG. 7. (Color online) The bias voltage dependence of the TMR in the case of (a) $\varepsilon/E_C = -2.8$ and (b) $\varepsilon/E_C = -1.2$ for different magnitude of the SMM's spin S. The other parameters are the same as in Fig. 2 with $J_S/E_C = -0.15$.

the number of states relevant for transport is much larger in the parallel configuration, there is an enhancement of the TMR [see Fig. 6(c)]. However, since the spin accumulation is now smaller than in the case of ferromagnetic J_S for odd occupation of the molecule, lower TMR is consequently observed. On the other hand, when the system is occupied by a single electron, the twofold degenerate ground state is $|1,0,\pm S \mp \frac{1}{2}\rangle$. With increasing the bias voltage, in the antiparallel configuration, strong spin accumulation develops, with occupation probability of state $|1,0,-S+\frac{1}{2}\rangle$ close to unity. Moreover, spin accumulation is also present in the case of parallel configuration, but it is smaller than in the antiparallel configuration. We note that this situation is now somewhat similar to the case of ferromagnetic J_S, except for spin states that are relevant for transport, which is in fact the key factor in observing a completely different behavior. In the case of ferromagnetic coupling, the spin accumulation developed in highest-weight spin states, while now this is not the case. The state $|1,0,-S+\frac{1}{2}\rangle$ is a linear combination of local states of the nanotube and appropriate spin multiplets of the molecular magnet. Consequently, while for $J_S > 0$ in the antiparallel configuration the system was trapped in a single state, which led to the suppression of transport and resulted in negative TMR, here we observe an enhancement of the TMR.

The effect of both TMR enhancement and negative TMR strongly depends on the magnitude of SMM's spin S. This is presented in Fig. 7, which shows the bias voltage dependence of the TMR for the corresponding two values of ε and for different S, as indicated in the figure. In the case of $\varepsilon/E_C = -2.8$, for $S = 0$, the TMR is rather low in the low bias voltage regime. With increasing the molecule's spin however it starts increasing and becomes larger than $\mathrm{TMR}^{\mathrm{Jull}}$ for $S = \frac{3}{2}$. However, further increase of S results in suppression of the TMR, such that for $S = \frac{5}{2}$ its behavior resembles that in the case of $S = 0$, see Fig. 7(a). The reason for it is again related to excitation energies, which become modified by changing the value of spin S. It turns our that for $S = \frac{3}{2}$, in the parallel configuration, the states $|2,0,\pm S\rangle$ are relevant for transport, while in the antiparallel configuration, due to strong nonequilibrium spin accumulation, a single state $|2,0,-S\rangle$ is responsible for the current flow. With increasing the magnitude of spin, nonequilibrium spin accumulation becomes decreased and occupation probability of states $|1,1\pm S \mp 1\rangle$ increases. This leads to the suppression of TMR and to its related nonmonotonic dependence on S.

When $\varepsilon/E_C = -1.2$, the system is singly occupied and the TMR becomes negative with increasing the value of spin S, see Fig. 7(b). This is related to the fact that in the antiparallel configuration the nonequilibrium spin accumulation in states $|1,0,\pm S \mp \frac{1}{2}\rangle$ increases with increasing S and, since these states are superpositions of local spin states, the thermally activated current becomes enhanced. As a consequence, one finds $I^{\mathrm{AP}} > I^{\mathrm{P}}$ and the TMR becomes negative. Interestingly, nonequilibrium spin accumulation also develops in the parallel configuration and becomes enhanced with increasing S. This is why for the largest value of S considered in Fig. 7(b), the TMR gets decreased.

We note that in the case of $\delta > J$, i.e., when the evenly occupied isolated nanotube is in the spin singlet state, the

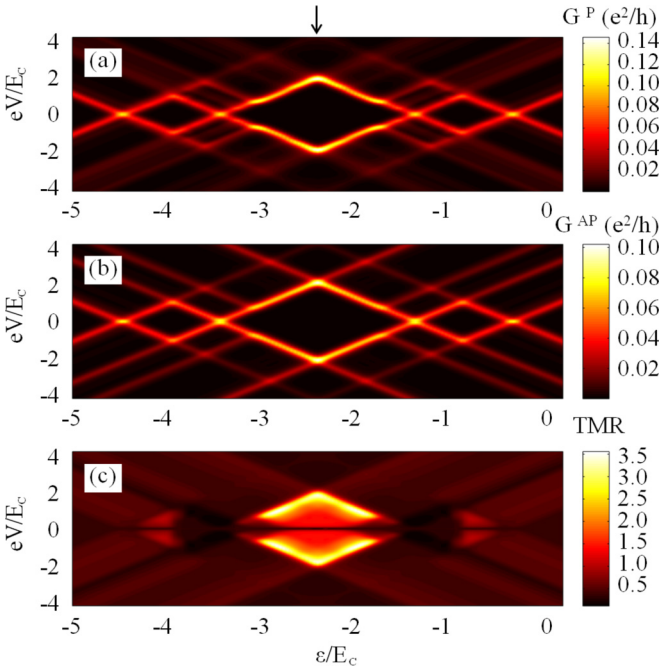

FIG. 8. (Color online) The bias and gate voltage dependence of the differential conductance in (a) the parallel and (b) antiparallel magnetic configuration and (c) the resulting TMR calculated in the case of ferromagnetic exchange coupling ($J_S > 0$) between the nanotube and molecular magnet. The parameters are the same as in Fig. 2 with $\delta/E_C = 0$.

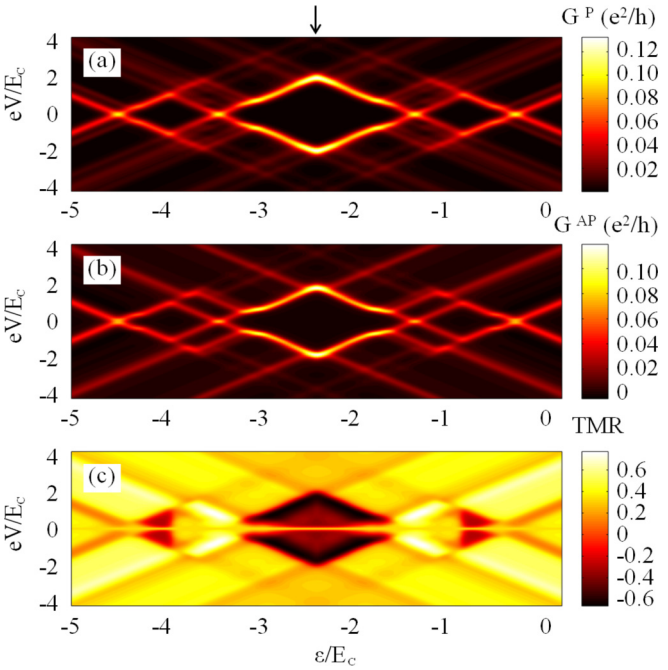

FIG. 9. (Color online) The same as in Fig. 8 calculated in the case of antiferromagnetic exchange coupling ($J_S < 0$) between CNT and SMM, $J_S/E_C = -0.15$.

type of exchange coupling J_S results in completely different behavior of spin-resolved transport characteristics. When the nanotube is occupied by two electrons, for (anti)ferromagnetic J_S, the TMR becomes (large and positive) negative. The difference is even more pronounced in the case of the odd occupancy of the nanotube. In the case of ferromagnetic J_S the TMR is then greatly enhanced (with values much exceeding the Julliere value), while for antiferromagnetic J_S the TMR becomes negative. Thus, by analyzing the tunnel magnetoresistance behavior one may extract additional information about the type of exchange coupling between the nanotube and the attached molecular magnet.

B. Results in the case of $J > \delta$

When $J > \delta$, the sequence of ground states of an isolated nanotube as a function of ε is different. Now the two-electron state is a spin triplet, with electrons occupying different orbital levels. Clearly the type of exchange interaction between the nanotube and molecule will play an important role, especially in the two-electron triplet regime. To assure that the condition $J > \delta$ is fulfilled, in the following we assume that there is no energy mismatch between the two subbands of the nanotube, i.e., we set $\delta = 0$.

The bias and gate voltage dependence of the differential conductance in both magnetic configurations and the TMR in the case of ferromagnetic exchange interaction J_S is shown in Fig. 8. Figures 8(a) and 8(b) present the Coulomb stability diagrams in the parallel and antiparallel configurations. Similarly to the case of $\delta > J$, one generally finds $G^{\mathrm{P}} > G^{\mathrm{AP}}$. Moreover, it can be seen that the size of the diamonds is now changed. The middle diamond (with two electrons) is much larger than the two neighboring ones. With similar assumptions as made when deriving Eq. (8), one can find the respective resonance energies where two charge states become degenerate. They can be expressed as

$$\varepsilon_{12} = -\frac{3E_C}{2} - \delta + \frac{J_S S}{2}, \qquad \varepsilon_{23} = -\frac{5E_C}{2} - 2J - \frac{J_S S}{2}, \tag{10}$$

while ε_{01} and ε_{34} are given by Eq. (8). The middle of the stability diagram is again for $\varepsilon_m = -2E_C - J - \delta/2$, however, due to different parameters ($\delta = 0$), it occurs for a different value of ε, namely, $\varepsilon/E_C = -2.4$, as indicated by an arrow in Fig. 8. The size of the diamonds with an odd number of electrons is given by $\varepsilon_{01} - \varepsilon_{21} = E_C + \delta$, while the size of the middle diamond is $\varepsilon_{12} - \varepsilon_{23} = E_C - \delta + 2J + J_S S$. Thus, changing the magnitude of SMM's spin or exchange coupling J_S affects the size of the second diamond, while the first and third Coulomb diamonds remain unaltered.

The dependence of the TMR on bias and gate voltages is shown in Fig. 8(c). As already mentioned, most spectacular behavior of the TMR can be seen in diamond with two electrons, when the isolated nanotube is in the triplet state. Ferromagnetic exchange interaction with the molecule increases the spin of the system by $s = 1$. Because of that, transport is mainly determined by the highest-weight spin states, which consequently results in highly nontrivial behavior of the TMR. In addition, one can also notice small enhancement of the TMR in the case of Coulomb blockade with an odd number of electrons, see Fig. 8(c).

Before discussing in more detail the mechanism leading to the enhanced TMR, let us first analyze the general transport behavior in the case of antiferromagnetic exchange coupling, where a completely different dependence of the TMR is observed. By directly comparing the behavior of the TMR in the case of $J_S > 0$ and $J_S < 0$, it will then be more straightforward to grasp the main features and mechanisms responsible for those effects.

The differential conductance in both magnetic configurations and the TMR as a function of bias and gate voltages in the case of antiferromagnetic J_S are shown in Fig. 9. As before, one can find the conditions for the resonant energies ε_{qq+1}. The energies ε_{01} and ε_{34} are given by Eq. (9), while to get ε_{12} and ε_{23} one needs to find the condition for degeneracy between antiferromagnetic states with one electron of spin $S - \frac{1}{2}$ and with two electrons of total spin $S - 1$. The SMM-dependent part of these formulas is however quite cumbersome, therefore we will not present it here.

One can see that the bias and gate voltage dependence of the differential conductance is qualitatively similar to that shown in Fig. 8 with a large middle Coulomb diamond and small neighboring diamonds. The main differences can be seen in the behavior of the TMR. Very interestingly, now in the two-electron Coulomb blockade regime, one finds negative TMR, which reaches values much below zero, $\mathrm{TMR} \approx -\mathrm{TMR}^{\mathrm{Jull}}$. Moreover, suppressed TMR can be also observed in the transport regime where the system is occupied by an odd number of electrons. In other transport regimes, the TMR is generally positive and not particularly large.

Since the most spectacular and nontrivial behavior of the TMR is observed in the case when the system is occupied by two electrons, let us now analyze the relevant cross sections of Figs. 8 and 9. The bias voltage dependence of the current and differential conductance in both magnetic configurations as well as the TMR is shown in Fig. 10 in the case of $\varepsilon = \varepsilon_m$, i.e., in the middle of the Coulomb blockade with two electrons (as indicated by the arrows in Figs. 8 and 9). The left column presents the results for ferromagnetic exchange coupling, while the right column corresponds to the case of antiferromagnetic coupling. One can see that while the current voltage characteristics are qualitatively similar, with Coulomb steps occurring at comparable threshold voltages, the TMR behavior is completely different. Besides, one can also notice a small shift of the peak in differential conductance in the antiparallel configuration compared to the parallel one. More precisely, in the case of ferromagnetic J_S the peak is shifted upwards, while for antiferromagnetic J_S this peak is shifted downwards.

Let us now focus on the behavior of the TMR. For ferromagnetic exchange interaction, the ground state of the system is twofold degenerate and given by the highest-weight spin states, $|1,1,\pm S \pm 1\rangle$. In the parallel configuration, only these two states, with equal probabilities, take part in transport. However, in the antiparallel configuration, due to nonequilibrium spin accumulation, the system becomes trapped in state $|1,1,-S-1\rangle$, which suppresses the thermally activated transport. As a result, the TMR becomes greatly enhanced, with values much exceeding the Julliere value, see Fig. 10(c). A completely opposite situation is observed in the case of antiferromagnetic exchange interaction $J_S < 0$. Now

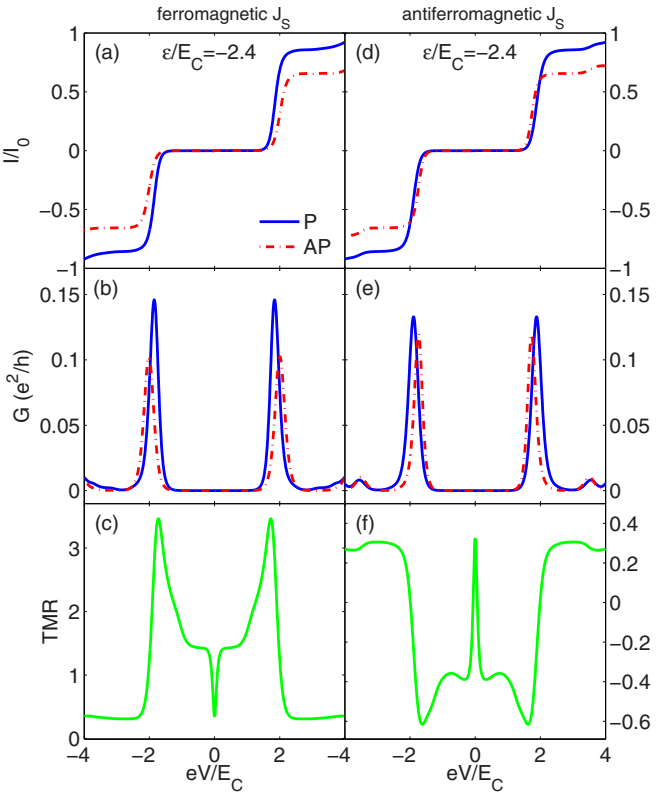

FIG. 10. (Color online) The bias voltage dependence of (a) and (d) the current, (b) and (e) differential conductance in both magnetic configurations, and (c) and (f) the TMR in the case of ferromagnetic ($J_S > 0$, left column) and antiferromagnetic ($J_S < 0$, right column) exchange interaction. The other parameters are the same as in Fig. 8 with $|J_S|/E_C = 0.15$ and $\varepsilon/E_C = -2.4$.

the system has antiferromagnetic twofold degenerate ground state $|1,1,\pm S \mp 1\rangle$. Again, with increasing the bias voltage, nonequilibrium spin accumulation builds up in the antiparallel configuration, such that the state $|1,1,-S+1\rangle$ is almost fully occupied. However, because this is not highest-weight spin state but a state which is a superposition of some local spin states, the thermally activated sequential transport then becomes enhanced in the antiparallel configuration compared to the parallel one. As a consequence, $I^{\mathrm{AP}} > I^{\mathrm{P}}$, giving rise to negative TMR. Note that the effect of negative TMR is now more pronounced compared to the case of $\delta > J$, such that TMR reaches almost $\mathrm{TMR} \approx -\mathrm{TMR}^{\mathrm{Jull}}$, see Fig. 10(f).

Finally, we analyze how the magnitude of the molecular magnet's spin S affects the above mentioned effects. The corresponding bias voltage dependence of the TMR in the case of both ferromagnetic and antiferromagnetic exchange interaction is shown in Fig. 11 for $\varepsilon/E_C = -2.4$. It is clearly visible how the effects of both enhanced TMR and negative TMR gradually develop with increasing S. For $J_S > 0$, one finds $\mathrm{TMR} > \mathrm{TMR}^{\mathrm{Jull}}$, even in the case of $S = 0$ [38]. Further increase of S enhances the TMR, such that for $S \geqslant 1$ one finds $\mathrm{TMR} \gg \mathrm{TMR}^{\mathrm{Jull}}$, see Fig. 11(a). On the other hand, for $J_S < 0$, the enhanced TMR for $S = 0$ becomes suppressed with increasing the magnitude of spin S, such that for $S \geqslant 1$ the TMR becomes negative, see Fig. 11(b). The TMR dependence

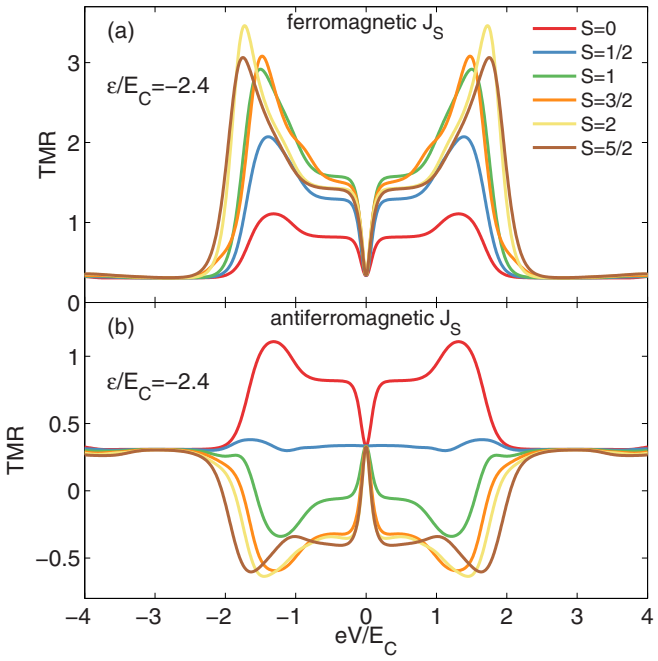

FIG. 11. (Color online) The tunnel magnetoresistance as a function of the bias voltage in the case of (a) ferromagnetic and (b) antiferromagnetic exchange interaction calculated for $\varepsilon/E_C = -2.4$ and for different values of SMM's spin, as indicated. The other parameters are the same as in Fig. 8 with $|J_S|/E_C = 0.15$.

on spin S reflects the fact that the effect of nonequilibrium spin accumulation becomes enhanced with increasing S and, thus, the above-described mechanisms responsible for corresponding TMR behavior become even more effective. Here, however, it is crucial whether the spin accumulation develops in highest-weight spin states or in states with lower spin values. In the former case this leads to greatly enhanced TMR, while in the latter case negative TMR can occur.

IV. CONCLUSIONS

In this paper we have considered the spin-resolved transport properties of a single-wall carbon nanotube quantum dot, with an attached single molecular magnet, coupled to external ferromagnetic leads. By using the real-time diagrammatic technique in the lowest-order perturbative expansion with respect to the tunnel coupling, we have determined the bias and gate voltage dependence of the current, differential conductance, and the tunnel magnetoresistance, which is associated with a change of magnetic configuration from a parallel into an antiparallel one. In particular, we have analyzed two possible scenarios for a carbon nanotube shell filling sequence, which can be realized depending on nanotube intrinsic parameters. In the first scenario, the doubly occupied ground state of the nanotube is a spin singlet, while in the second scenario, the doubly occupied ground state becomes a spin triplet. We have shown that the sequence of the nanotube's ground states and the type of exchange interaction J_S between the nanotube and molecule have a strong influence on the spin-resolved transport properties of the system, which is most visible in the TMR.

In the case when the two-electron ground state of the nanotube is spin singlet, in the low bias voltage regime we found negative (enhanced) TMR in the case of ferromagnetic (antiferromagnetic) exchange coupling J_S. On the other hand, when the nanotube occupancy is odd, an opposite situation was observed—an enhanced (negative) TMR was found in the case of ferromagnetic (antiferromagnetic) J_S. An even more spectacular dependence of the TMR on the type of exchange interaction J_S was observed in the case when the two-electron ground state of the nanotube was spin triplet. Then, in the case of ferromagnetic exchange interaction, a greatly enhanced TMR developed, while for antiferromagnetic J_S, a negative TMR was observed. The mechanisms leading to the above mentioned effects are generally associated with nonequilibrium spin accumulation that builds up in the antiparallel configuration. A crucial point is whether the spin accumulation develops in highest-weight spin states or in states with lower spin values. Spin accumulation in the highest-weight spin states generally leads to the suppression of conductance in the antiparallel configuration, which results in an enhancement of the TMR. On the other hand, the spin accumulation in states with lower spins, enhances thermally activated transport in the antiparallel configuration, leading to suppressed or even negative TMR.

In addition, we have also studied how the effects of both enhanced and suppressed (negative) TMR depend on the magnitude of the molecular magnet's spin S. A general observation is that those effects become enhanced when attaching molecules with larger spin, which is associated with the fact that the nonequilibrium spin accumulation becomes stronger with increasing the magnitude of SMM's spin S.

ACKNOWLEDGMENTS

We acknowledge discussions with M. Misiorny. This work was supported by the National Science Centre in Poland through the Project No. DEC-2013/10/E/ST3/00213.

[1] H. Grabert and M. H. Devoret, *Single Charge Tunneling: Coulomb Blockade Phenomena in Nanostructures*, NATO ASI Series B: Physics 294 (Plenum, New York, 1992).
[2] D. D. Awschalom, D. Loss, and N. Samarth, *Semiconductor Spintronics and Quantum Computation* (Springer, Berlin, 2002).
[3] S. Andergassen, V. Meden, H. Schoeller, J. Splettstoesser, and M. R. Wegewijs, Nanotechnology **21**, 272001 (2010).
[4] J. J. Parks, A. R. Champagne, T. A. Costi, W. W. Shum, A. N. Pasupathy, E. Neuscamman, S. Flores-Torres, P. S. Cornaglia, A. A. Aligia, C. A. Balseiro, G. K. L. Chan, H. D. Abruna, and D. C. Ralph, Science **328**, 1370 (2010).
[5] M. Urdampilleta, S. Klyatskaya, J.-P. Cleuziou, M. Ruben, and W. Wernsdorfer, Nat. Mater. **10**, 502 (2011).
[6] M. Ganzhorn, S. Klyatskaya, M. Ruben, and W. Wernsdorfer, Nat. Nanotech. **8**, 165 (2013).
[7] J. Kondo, Prog. Theor. Phys. **32**, 37 (1964).
[8] D. Goldhaber-Gordon, H. Shtrikman, D. Mahalu, D. Abusch-Magder, U. Meirav, and M. A. Kastner, Nature (London) **391**, 156 (1998).

[9] S. Cronenwett, T. H. Oosterkamp, and L. P. Kouwenhoven, Science **281**, 540 (1998).
[10] J. Barnaś and A. Fert, Phys. Rev. Lett. **80**, 1058 (1998).
[11] A. N. Pasupathy, R. C. Bialczak, J. Martinek, J. E. Grose, L. A. K. Donev, P. L. McEuen, and D. C. Ralph, Science **306**, 86 (2004).
[12] I. Weymann, J. König, J. Martinek, J. Barnaś, and G. Schön, Phys. Rev. B **72**, 115334 (2005).
[13] S. Sahoo, T. Kontos, J. Furer, C. Hoffmann, M. Gräber, A. Cottet, and C. Schönenberger, Nat. Phys. **1**, 99 (2005).
[14] J. R. Hauptmann, J. Paaske, and P. E. Lindelof, Nat. Phys. **4**, 373 (2008).
[15] M. Gaass, A. K. Hüttel, K. Kang, I. Weymann, J. von Delft, and C. Strunk, Phys. Rev. Lett. **107**, 176808 (2011).
[16] J. Barnaś and I. Weymann, J. Phys. Condens. Matter **20**, 423202 (2008).
[17] S. A. Wolf, D. D. Awschalom, R. A. Buhrman, J. M. Daughton, S. von Molnar, M. L. Roukes, A. Y. Chtchelka, and D. M. Treger, Science **294**, 1488 (2001).
[18] S. Maekawa and T. Shinjo, *Spin Dependent Transport in Magnetic Nanostructures* (Taylor and Francis, London, 2002).
[19] I. Zutic, J. Fabian, and S. Das Sarma, Rev. Mod. Phys. **76**, 323 (2004).
[20] W. Rudziński and J. Barnaś, Phys. Rev. B **64**, 085318 (2001).
[21] M. Braun, J. König, and J. Martinek, Phys. Rev. B **70**, 195345 (2004).
[22] M. Misiorny, I. Weymann, and J. Barnaś, Phys. Rev. B **79**, 224420 (2009).
[23] D. Gatteschi, R. Sessoli, and J. Villain, *Molecular Nanomagnets* (Oxford University Press, New York, 2006).
[24] L. Bogani and W. Wernsdorfer, Nat. Mater. **7**, 179 (2008).
[25] S. Sanvito, Chem. Soc. Rev. **40**, 3336 (2011).
[26] M. Misiorny and J. Barnaś, Europhys. Lett. **78**, 27003 (2007).
[27] M. Misiorny, I. Weymann, and J. Barnaś, Europhys. Lett. **89**, 18003 (2010).
[28] H. Hao, X. H. Zheng, Z. X. Dai, and Z. Zeng, Appl. Phys. Lett. **96**, 192112 (2010).
[29] M. Misiorny, I. Weymann, and J. Barnaś, Phys. Rev. B **84**, 035445 (2011).
[30] M. Misiorny, I. Weymann, and J. Barnaś, Phys. Rev. Lett. **106**, 126602 (2011).
[31] F. R. Renani and G. Kirczenow, Phys. Rev. B **87**, 121403(R) (2013).
[32] E. Cremades, C. D. Pemmaraju, S. Sanvito, and E. Ruiz, Nanoscale **5**, 4751 (2013).
[33] W. Luo, R. Q. Wang, L. B. Hu, and M. Yang, Chin. Phys. B **22**, 047201 (2013).
[34] M. Misiorny, M. Hell, and M. Wegewijs, Nat. Phys. **9**, 801 (2013).
[35] D. Loss and D. P. DiVincenzo, Phys. Rev. A **57**, 120 (1998).
[36] C. Chappert, A. Fert, and V. D. F. Nguyen, Nat. Mater. **6**, 813 (2007).
[37] A. Cottet and M.-S. Choi, Phys. Rev. B **74**, 235316 (2006).
[38] I. Weymann, J. Barnaś, and S. Krompiewski, Phys. Rev. B **76**, 155408 (2007).
[39] I. Weymann, J. Barnaś, and S. Krompiewski, Phys. Rev. B **78**, 035422 (2008); I. Weymann, S. Krompiewski, and J. Barnaś, Acta Phys. Pol. A **115**, 296 (2009).
[40] C. Schenke, S. Koller, L. Mayrhofer, and M. Grifoni, Phys. Rev. B **80**, 035412 (2009).
[41] I. Weymann and J. Barnaś, Phys. Rev. B **82**, 165450 (2010).
[42] S. Koller, M. Grifoni, and J. Paaske, Phys. Rev. B **85**, 045313 (2012).
[43] J. Samm, J. Gramich, A. Baumgartner, M. Weiss, and C. Schönenberger, J. Appl. Phys. **115**, 174309 (2014).
[44] A. Dirnaichner, M. Grifoni, A. Prüfling, D. Steininger, A. K. Hüttel, and Ch. Strunk, Phys. Rev. B **91**, 195402 (2015).
[45] H. Schoeller and G. Schön, Phys. Rev. B **50**, 18436 (1994).
[46] A. Thielmann, M. H. Hettler, J. König, and G. Schön, Phys. Rev. B **68**, 115105 (2003).
[47] A. Thielmann, M. H. Hettler, J. König, and G. Schön, Phys. Rev. Lett. **95**, 146806 (2005).
[48] Y. Oreg, K. Byczuk, and B. I. Halperin, Phys. Rev. Lett. **85**, 365 (2000).
[49] W. Liang, M. Bockrath, and H. Park, Phys. Rev. Lett. **88**, 126801 (2002).
[50] S. Sapmaz, P. Jarillo-Herrero, J. Kong, C. Dekker, L. P. Kouwenhoven, and H. S. J. van der Zant, Phys. Rev. B **71**, 153402 (2005).
[51] S. Moriyama, T. Fuse, M. Suzuki, Y. Aoyagi, and K. Ishibashi, Phys. Rev. Lett. **94**, 186806 (2005).
[52] C. Timm and F. Elste, Phys. Rev. B **73**, 235304 (2006).
[53] F. Elste and C. Timm, Phys. Rev. B **73**, 235305 (2006).
[54] A. Thielmann, M. H. Hettler, J. König, and G. Schön, Phys. Rev. B **71**, 045341 (2003).
[55] M. Julliere, Phys. Lett. A **54**, 225 (1975).
[56] D. V. Averin and Y. V. Nazarov, Phys. Rev. Lett. **65**, 2446 (1990).
[57] K. Kang and B. I. Min, Phys. Rev. B **55**, 15412 (1997).
[58] S. Mossin, L. Tran, D. Adhikar, M. Pink, F. W. Heinemann, J. Sutter, R. K. Szilagyi, K. Meyer, and D. J. Mindiola, J. Am. Chem. Soc. **134**, 13651 (2012).